Estimation of constituent properties of concrete materials with an artificial neural network based method

J Xue, J. Shao, Nicolas Burlion

▶ **To cite this version:**

J Xue, J. Shao, Nicolas Burlion. Estimation of constituent properties of concrete materials with an artificial neural network based method. Cement and Concrete Research, 2021, 150, 10.1016/j.cemconres.2021.106614 . hal-04508816

HAL Id: hal-04508816
https://hal.science/hal-04508816

Submitted on 22 Jul 2024

HAL is a multi-disciplinary open access archive for the deposit and dissemination of scientific research documents, whether they are published or not. The documents may come from teaching and research institutions in France or abroad, or from public or private research centers.

L'archive ouverte pluridisciplinaire **HAL**, est destinée au dépôt et à la diffusion de documents scientifiques de niveau recherche, publiés ou non, émanant des établissements d'enseignement et de recherche français ou étrangers, des laboratoires publics ou privés.

Distributed under a Creative Commons Attribution - NonCommercial 4.0 International License

Version of Record: https://www.sciencedirect.com/science/article/pii/S0008884621002635
Manuscript_49b6ca5229e1ead8e9a64c71c62bc617

Estimation of constituent properties of concrete materials with an artificial neural network based method

J. Xue[a,b], J.F. Shao [a,b]*, N. Burlion[b]

[a]College of Civil Engineering and Transportation, Hohai University, 210098 Nanjing, China

[b]University of Lille, CNRS, Centrale Lille, LaMcube, UMR9013, 59000 Lille

*Corresponding author: jian-fu.shao@polytech-lille.fr

Abstract: Multi-scale models are developed for heterogeneous concrete materials to estimate their macroscopic mechanical properties in terms of micro-structural data. One crucial challenge of those models is the identification of local properties of constituent phases. In this paper, we present an efficient method based on Artificial Neural Networks (ANN). Typical concrete materials are taken as example. A macroscopic analytical strength criterion is established from three steps of nonlinear homogenization procedure. The macroscopic strength of materials is determined as a function of the frictional coefficient and cohesion of solid cement particles at nanometer scale, intra-particle pores, inter-particle pores and aggregates (inclusions). The objective is to identify the nanoscopic frictional coefficient and cohesion of cement particle from measured macroscopic values of uniaxial compression and tensile strengths. For this purpose, a numerical method based on the ANN is developed. With the analytical macroscopic strength criterion, sensitivity studies are first realized to identify the most important micro-structural parameters influencing the macroscopic strength of concrete. A simplified analytical macroscopic strength criterion is then proposed. A large dataset is further constructed through the inversion of the analytical strength criterion by using the aggregates volume fraction, porosity, macroscopic uniaxial tensile and compressive strengths as input variables and the frictional coefficient and cohesion of cement particles as output unknowns. An ANN model containing four hidden layers and 100 neurons in each layer is constructed and

© 2021 published by Elsevier. This manuscript is made available under the CC BY NC user license
https://creativecommons.org/licenses/by-nc/4.0/

trained by using this dataset. Various types of validation of the ANN model are performed. It is found that the proposed ANN based model can effectively predict the frictional coefficient and cohesion of porous cement paste at the microscopic scale with a very good accuracy.

Keywords: Multi-scale modeling; homogenization; parameter identification; artificial neural network; concrete; heterogeneous materials

1. Introduction

Concrete materials are widely used in engineering structures. The characterization of short and long term physical and mechanical properties is crucial for the analysis of stability and durability of concrete structures. Like most engineering materials, concrete materials are heterogeneous composites with complex and multi-scale micro-structures. It is well-known that their macroscopic properties are inherently related to micro-structural compositions and evolutions at different scales. Based on experimental data, many macroscopic models have been developed for describing mechanical behaviors of concretes. In general, these models are not able to explicitly establish links between macroscopic properties and micro-structural parameters. To overcome this shortcoming, micro-mechanical approaches have been developed for estimating macroscopic mechanical properties of concrete composites in terms of microstructural parameters and constituent properties. In particular, by using nonlinear homogenization techniques, a number of analytical strength criteria have been established for heterogeneous materials containing pores and inclusions at different scales (Maghous et al., 2009; Shen et al., 2013; Shen et al. 2017; Shen et al. 2020). Basic on such criteria, full elastic-plastic models have been formulated by considering hardening or damage (Shen et al., 2012; Bignonnet et al., 2016; Shen and Shao, 2016; Shen et al. 2020a; Aldakheel, 2020). On the other hand, based on the full simulations of representative volume elements by using suitable numerical methods, different types of numerical homogenization techniques have also been developed for

the prediction of macroscopic responses of materials with complex micro-structures (Cao et al., 2018a; Cao et al. 2018b; Cao et al., 2020). A number of micromechanical models have been successively applied to cement-based materials (Ghorbanbeigi et al., 2016; Paiva et al., 2017; Konigsberger et al. 2018; Zhang et al., 2020).

For all these micro-mechanics based models, the estimation of macroscopic mechanical properties is inherently based on the description of microstructures and local mechanical properties of constituent phases. For instance, for concrete materials, typical microstructures are composed of cement paste (solid matrix), voids, inclusions and interface transition zones. In many previous models, the local plastic yield or strength criterion of the solid matrix is generally described the Drucker-Prager (DP) linear function which is characterized by frictional and cohesion coefficients. Therefore, the identification of such local mechanical properties at microscopic scales is the key issue of micro-mechanical approaches. Advanced multi-scale testing methods have been developed in order to realize direct measurement of local mechanical properties, for instance nanoindentation and micro-bending tests (Nemecek et al., 2016; Konigsberger et al., 2018; Qian et al., 2018; Lau et al., 2019). However, in most cases, these experimental techniques are so far used for the identification of local elastic properties and tensile strength at a given scale. It is not easy to apply these techniques at different scales. In most case, optimal inversion methods are usually adopted for the estimation of microscopic properties using macroscopic measurements. The efficiency of these methods is not fully guaranteed for cases of several parameters to be identified. More efficient and systematic methods should be developed.

During the recent years, machine-learning (ML) based methods have been rapidly developed in various engineering fields including materials science and technology. Indeed，based on a deep training, such fully data-driven methods have been proven to be a powerful and versatile problem-solving tool for both multi-scale characterization and design of different types of engineering materials and structures. For instance and without wanting to give an exhaustive review, anisotropic masonry

failure properties have been investigated with Artificial Neural Networks (Asteris and Plevris, 2017). Stochastic vulnerability of masonry structures has further been assessed (Asteris et al. 2019). ML based solutions have also been applied to mapping and holistic design of natural hydraulic lime mortars (Apostolopoulou et al. 2020). Some authors have proposed a hybrid combination of surrogate machine learning models to predict concrete compressive strength (Asteris et al. 2021). Peak particle velocity caused by blasting was predicted by using combinations of boosted-CHAID and SVM Models with various kernels (Zeng et al. 2021). In some recent studies, some authors have tried to estimate macroscopic strength of porous materials by using Artificial Neural Networks (Shen et al. 2020b).

Therefore, among different types of ML-based solutions, Artificial Neural Networks (ANN) are one of the mostly adopted methods. The ANN can accurately identify and learn underlying relationships between input and output data without considering explicit mathematical equations (Haykin, 2010). Besides, ANN-based solutions are viewed as an effective alternative to traditional statistical analysis techniques for function approximation and data fitting due to regardless of assumptions about mathematical models (Rahman and Zhang, 2018). This type of method has also been applied to identify constituent properties of concrete materials, for instance, to identify the nanoscopic elastic modulus of different phases of cementitious matrix (Ford et al. 2020), to get the abrasion performance of the fly ash-based geopolymer (Lau et al. 2019). Some authors have also used the ANN method to investigate the effect of carbon nanotubes on mechanical properties of novel cement formulations (Konstantopoulos et al., 2020).

However, in most previous studies, the emphasis was put on the estimation of macroscopic physical and mechanical properties. Among studies on the identification of constituents mechanical properties, most are limited to elastic ones. Very few studies are available on the estimation of failure or strength properties of constituents. Moreover, in most previous studies, only one material scale was considered at the same time while concrete materials are multi-scale composites. Therefore, there is

clearly a need to perform further investigations on the identification of strength properties of constituents in multi-scale heterogeneous materials such as concrete. This is the main objective of this work.

For this purpose, based on the artificial neural networks (ANN) technique, a new numerical method is developed for the identification of local strength parameters of solid cement paste by taking into account simultaneously effects of pores and inclusions. In particular, an original strategy is developed by the combination of an ANN model with an analytical strength criterion issued from three steps of nonlinear homogenization. This one has the advantage of easily constructing a large data set by using analytical solutions, for the ANN model training and verification. The present paper is organized in three main parts. In Section 2, an analytical macroscopic strength criterion for concrete-like composites is presented. With this model, a sensitivity study is performed to identify the key microstructural parameters controlling the macroscopic strength of materials and to formulate a simplified analytical macroscopic strength criterion. The general procedure to build an ANN model is presented in Section 3. The ANN model is used in Section 4 for the prediction of the local friction and cohesion coefficients of porous cement phase at the microscopic scale. Its accuracy is clearly demonstrated through comparisons with analytical solutions. Some concluding remarks are finally presented in Section 5.

2. Sensitivity analysis of microstructural parameters

In order to identify the key microstructural parameters controlling the macroscopic strength of concrete materials, a sensitivity study is first performed. It is worth noticing that micro-structures of concrete materials are generally complex. For instances, different types of Calcium silicate hydrate (C-S-H) are formed in cement paste. Voids and inclusions of different sizes are distributed at different scales. The macroscopic mechanical properties of concrete materials are inherently affected by their local counterparts of constituent phases, their morphology, porosity and volumetric fraction of inclusions. Further, interface transition zones (ITZ) are created around aggregates and pores. They can significantly affect the macroscopic

mechanical properties of materials. It is hard to consider all these micro-structural parameters at the same time.

In this study, the following methodology is adopted. We shall take advantage of some analytical solutions issued from rigorous nonlinear homogenization techniques to establish explicit relations between macroscopic strength of concrete and local strength properties of cement paste, pores and inclusions. In this way, the macroscopic strength criteria can be formulated in a closed form. Typical strength parameters such as uniaxial compression and tension strengths can be very easily calculated with any numerical simulations. Therefore, in view of ANN training, it is very easy to construct a large data set with very simple calculations with the help of analytical strength criteria. However, the shortcoming of this study is that the micro-structural morphology of concrete materials should be simplified in order to establish analytical strength criteria. For instance, it is mathematically very difficult to derive analytical strength criteria by considering pores, inclusions and ITZ at the same time. As a consequence, the effect of ITZ is omitted in this study. It could be taken into account in future investigations by using direct numerical simulations of concrete micro-structures to construct data set.

With this basic idea, the objective of sensitivity study presented here is to hierarchize the influences of different micro-structural parameters on macroscopic strength. Based on this study, a simplified formulation of the macroscopic strength criterion is proposed.

2.1 Presentation of analytical strength criterion and problem statement

Based on the methodology presented above, we consider here concrete or rock like composites containing two populations of pores and a family of inclusions at three separate scales. The representative volume element (RVE) of heterogeneous material is illustrated in Fig. 1.

At the macroscopic scale (cm), the material is represented by a homogenized equivalent medium (HEM) whose strength properties are to be predicted. At the mesoscopic scale (mm), mineral inclusions (quartz and calcite grains, aggregates etc.)

175 are distributed in a quasi-continuous matrix (for instance clay matrix or cement paste).
176 At the microscopic scale (μm), this matrix phase contains a family of (large) pores
177 (inter-particle pores of a few hundreds of nanometers to micrometers). At the
178 nanoscopic scale (nm), small pores (intra-particle pores of a few nanometers) are
179 embedded inside solid particles.
180

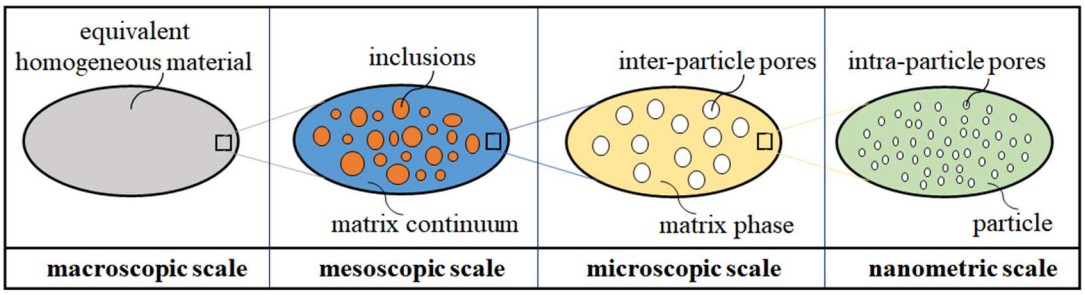

Fig. 1. RVE of heterogeneous materials with two families of pores and inclusions.

181

182 It is assumed that the solid phase at the nanoscopic scale is described by a
183 pressure-sensitive Drucker-Prager type yield or strength criterion:

$$F^s = \tilde{\sigma}_d + T(\tilde{\sigma}_m - h) \leq 0 \tag{1}$$

184 where $\tilde{\boldsymbol{\sigma}}$ denotes the stress tensor of the solid phase. $\tilde{\sigma}_m = tr\tilde{\boldsymbol{\sigma}}/3$ is the mean stress.
185 $\tilde{\sigma}_d$ is the deviatoric stress defined as $\tilde{\sigma}_d = \sqrt{\tilde{\boldsymbol{\sigma}}' : \tilde{\boldsymbol{\sigma}}'}$, with $\tilde{\boldsymbol{\sigma}}'$ being the deviatoric
186 part of the stress tensor. The parameter T denotes the frictional coefficient and h the
187 hydrostatic tensile strength (also related to internal cohesion) of the solid phase at the
188 nanoscopic scale. By performing three steps of nonlinear homogenization with the
189 modified secant method (Maghous et al., 2009; Shen et al., 2013, Cao et al., 2020),
190 one obtains the following close-form of the macroscopic strength criterion:

$$F = \frac{A + \frac{2B\rho}{3}}{1 + \frac{3\rho}{2} - \frac{5\rho}{6\left(\frac{A}{B} + 1\right)}}\Sigma_d^2 + B\Sigma_m^2 + C\Sigma_m - \left(D + \frac{4BD + C^2}{6A}\rho\right) = 0 \tag{2}$$

191 with the following coefficients:

$$\begin{aligned} &A = \frac{1+\frac{2f}{3}}{T^2}\left(\frac{6T^2-13f-6}{4T^2-12f-9}\phi + 1\right),\ B = \frac{\frac{3}{2}+f}{T^2}\phi + \frac{3f}{2T^2} - 1, \\ &C = 2(1-f)(1-\phi)h,\ D = (1-f)^2(1-\phi)^2h^2. \end{aligned} \tag{3}$$

In this criterion, Σ is the macroscopic stress tensor, $\Sigma_m = tr\Sigma/3$ is the mean stress and $\Sigma_d = \sqrt{\Sigma' : \Sigma'}$ is the deviatoric stress with Σ' being the macroscopic deviatoric stress tensor. ρ represents the volume fraction of inclusions, ϕ is the large porosity at the microscopic scale while f being the small porosity at the nanometric scale.

The strength criterion (2) is now applied to the case of uniaxial stress loading. At failure state, one has $\Sigma_d = R$, $\Sigma_m = (-1/3)R$, with R being the failure strength which can be determined by the following relation.

$$\left(\frac{A + \frac{2B\rho}{3}}{1 + \frac{3\rho}{2} - \frac{5\rho}{6\left(\frac{A}{B} + 1\right)}} + \frac{B}{9} \right) R^2 - \frac{C}{3} R - \left(D + \frac{4BD + C^2}{6A} \rho \right) = 0 \qquad (4)$$

The above quadratic equation admits one positive and one negative solution, which respectively corresponds to the uniaxial tensile strength R_t and the uniaxial compression strength R_c. Therefore, by knowing the microstructural parameters parameters (ρ, ϕ, f) and the nanoscopic strength properties of solid cement particles (T, h), it is easy to calculate the two basic macroscopic strength parameters (R_c, R_t). But the objective here is to solve the corresponding inverse problem, consisting of identifying the values of the nanoscopic strength properties of solid cement particles (T, h) from the easily measurable macroscopic strength parameters (R_c, R_t).

2.2 Sensitivity analysis

Before going to the resolution of the inverse problem, a sensitivity analysis is first realized. The objective is to quantify the dependency of two macroscopic strength parameters (R_c, R_t) on the three microstructural parameters (ρ, ϕ, f) in order to define their relative impact on the macroscopic strength.

Different types of methods are available for performing sensitivity analysis, including one-at-a-time method (OAT) (Czitrom, 1999; Saltelli and Annoni, 2010), the derivative-based local approaches (Cacuci et al., 2005; Griewank and Walther, 2008), the regression analysis (Galton et al., 1989), the variance-based methods

(so-called Sobol method) (Sobol, 2001; Saltelli, 2002; Saltelli et al., 2010), the variogram analysis of response surfaces (VARS) (Razavi and Gupta, 2016a; Razavi and Gupta, 2016b), the Scatter plots (Paruolo et al., 2013) and others. The Sobol method is used in this paper because it can measure the sensitivity across the whole input space (i.e., the global method), handle nonlinear responses, and measure the impact of interactions in non-additive systems (Saltelli, 2002).

For the simplicity of presentation, only the influence of input parameters (ρ, ϕ, f, T, h) on the uniaxial compression strength R_c using Eq. (4) is analyzed here. For this purpose, the relationship between R_c and the input parameters is written as:

$$R_c = g(\boldsymbol{X}) \tag{5}$$

where $\boldsymbol{X} = [\rho, \phi, f, T, h]$. The calculation sequence of sensitivity analysis is as follows.

Step 1: Randomly generate two independent 1000×5 sample matrices, i.e. each row is a sample point in the hyperspace of 5 dimensions. The value range of the parameter is: $\rho\epsilon[0,1]$, $\phi\epsilon[0,1]$, $f\epsilon[0,0.5]$, $T\epsilon[0,1]$, $h\epsilon[0,80]$. The generated matrices are recorded as $\boldsymbol{A}$, $\boldsymbol{B}$.

$$\boldsymbol{A} = \begin{bmatrix} \rho_1 & \phi_1 & f_1 & T_1 & h_1 \\ \rho_2 & \phi_2 & f_2 & T_2 & h_2 \\ \vdots & \vdots & \vdots & \vdots & \vdots \\ \rho_{1000} & \phi_{1000} & f_{1000} & T_{1000} & h_{1000} \end{bmatrix} \tag{6}$$

$$\boldsymbol{B} = \begin{bmatrix} \rho_1^* & \phi_1^* & f_1^* & T_1^* & h_1^* \\ \rho_2^* & \phi_2^* & f_2^* & T_2^* & h_2^* \\ \vdots & \vdots & \vdots & \vdots & \vdots \\ \rho_{1000}^* & \phi_{1000}^* & f_{1000}^* & T_{1000}^* & h_{1000}^* \end{bmatrix} \tag{7}$$

Step 2: Build 5 further 1000×5 matrices $\boldsymbol{A}_B^{(i)}$, with $i = 1, 2, \ldots, 5$, such that the i-th column of $\boldsymbol{A}_B^{(i)}$ is equal to the i-th column of $\boldsymbol{B}$, and the remaining columns are from $\boldsymbol{A}$. For instance $\boldsymbol{A}_B^{(3)}$ is as follows:

$$\boldsymbol{A}_B^{(3)} = \begin{bmatrix} \rho_1 & \phi_1 & f_1^* & T_1 & h_1 \\ \rho_2 & \phi_2 & f_2^* & T_2 & h_2 \\ \vdots & \vdots & \vdots & \vdots & \vdots \\ \rho_{1000} & \phi_{1000} & f_{1000}^* & T_{1000} & h_{1000} \end{bmatrix} \tag{8}$$

Step 3: Calculate the estimators by the method proposed in (Janson, 1999; Saltelli et al. 2010) with Eqs. (9)-(11). $(\boldsymbol{A})_j$ denotes the j-th row of the matrix $\boldsymbol{A}$, $(\boldsymbol{B})_j$ is the j-th row of the matrix $\boldsymbol{B}$, and $\left(\boldsymbol{A}_B^{(i)}\right)_j$ represents the j-th row of the matrix $\boldsymbol{A}_B^{(i)}$.

$$V_{Xi}\left(E_{\boldsymbol{X}\sim i}(Y|X_i)\right) = \frac{1}{1000}\sum_{j=1}^{1000} g(\boldsymbol{B})_j\left(g\left(\boldsymbol{A}_B^{(i)}\right)_j - g(\boldsymbol{A})_j\right) \tag{9}$$

$$E_{\boldsymbol{X}\sim i}\left(V_{Xi}(Y|\boldsymbol{X}_{\sim i})\right) = \frac{1}{2000}\sum_{j=1}^{1000}\left(g(\boldsymbol{A})_j - g\left(\boldsymbol{A}_B^{(i)}\right)_j\right)^2 \tag{10}$$

$$V(Y) = \frac{1}{1000}\sum_{j=1}^{1000} g(\boldsymbol{A})_j^2 - \left(\frac{1}{N}\sum_{j=1}^{N} g(\boldsymbol{A})_j\right)^2 \tag{11}$$

Step 4: Calculate the sensitivity indices using the estimators of step 3. The Sobol sensitivity index is defined as the ratio of partial variance to total variance (Sobol, 2001). The first and total sensitivity index is given by Eqs. (12) and (13).

$$S_i = \frac{V_{Xi}\left(E_{\boldsymbol{X}\sim i}(Y|X_i)\right)}{V(Y)} \tag{12}$$

$$S_{Ti} = 1 - \frac{V_{\boldsymbol{X}\sim i}\left(E_{Xi}(Y|\boldsymbol{X}_{\sim i})\right)}{V(Y)} = \frac{E_{\boldsymbol{X}\sim i}\left(V_{Xi}(Y|\boldsymbol{X}_{\sim i})\right)}{V(Y)} \tag{13}$$

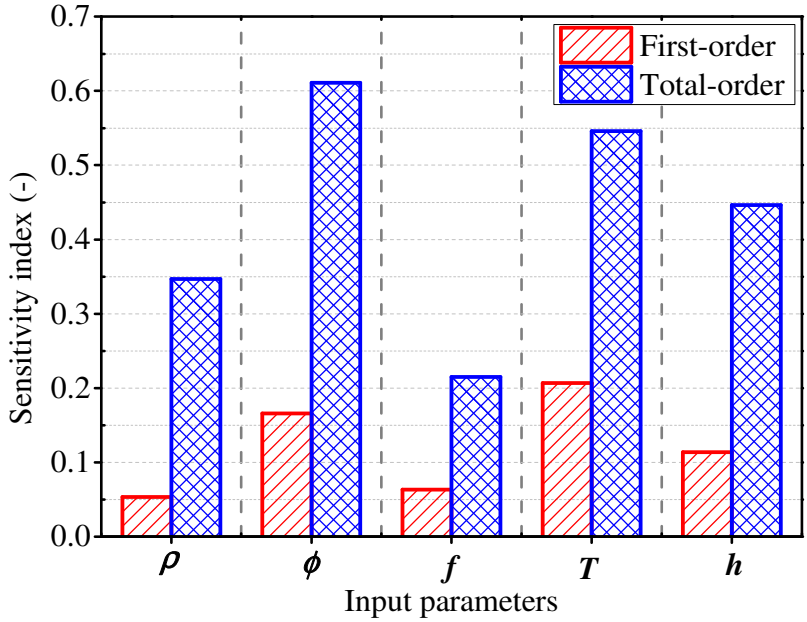

Fig. 2. Results of first-order and total-order index for input parameters.

The first-order and total-order indexes of five input parameters based on the Sobol method are presented in Fig. 2. Regarding the first-order sensitivity index, the three most relevant input features in order are $T > \phi > h$, while the two most non-significant features in order is $f > \rho$. For the total-order sensitivity index, the relevant input features in order are $\phi > T > h > \rho > f$. At the same time, there is a drastic difference between the first-order and total-order indexes for the same parameter. These results are consistent with the fact that the total-order sensitivity index considers the interaction among the input variables. According to the results obtained, one can consider that the small porosity f has the least influence on the macroscopic uniaxial compression strength. Very similar results can be obtained for the uniaxial tensile strength.

2.3 Simplification of analytical strength criterion

Based on the sensitivity study presented above, it seems that the effect of the nanoscopic porosity f on the macroscopic strength is relatively small. On the other hand, the porosity at the nanoscopic scale is also not easy to be accurately measured. In order to facilitate the solution of inverse problem, the microstructure of heterogeneous materials is simplified into three representative scales instead of four scales shown in Fig. 1. It is physically assumed that the intra-particle pores are merged into the solid cement paste phase, as suggested in (Konigsberger et al., 2018). The simplified microstructure is illustrated in Fig. 3.

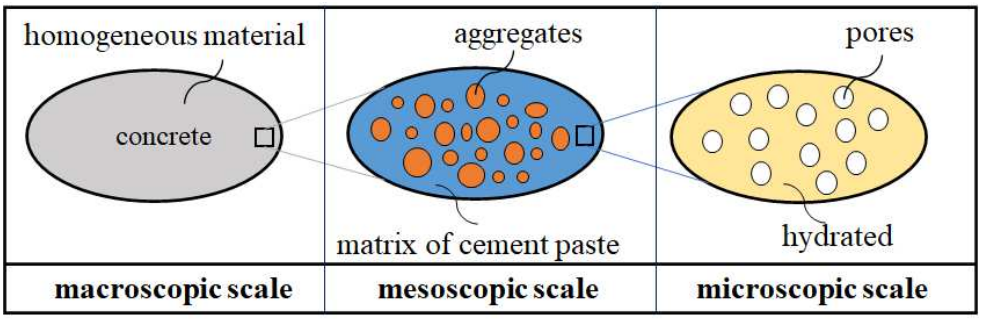

Fig. 3. Simplified RVE of concretes with pores and aggregates.

Accordingly, the macroscopic strength can be now obtained by making three steps of homogenization. This is equivalent to set $f = 0$ in the criterion (2) and the related coefficients (3). The simplified macroscopic strength criterion is expressed as:

$$F' = \frac{A' + \frac{2B'\rho}{3}}{1 + \frac{3\rho}{2} - \frac{5\rho}{6\left(\frac{A'}{B'} + 1\right)}}\Sigma_d^2 + B'\Sigma_m^2 + C'\Sigma_m - \left(D' + \frac{4B'D' + C'^2}{6A'}\rho\right) = 0 \quad (14)$$

with the following coefficients:

$$A' = \frac{1}{T'^2}\left(\frac{6T'^2 - 6}{4T'^2 - 9}\phi + 1\right),\ B' = \frac{3}{2T'^2}\phi - 1,$$
$$C' = 2(1-\phi)h',\ D' = (1-\phi)^2 h'^2. \quad (15)$$

It is worth noticing that in the initial strength criterion (2), the parameters T and h respectively represents the frictional and cohesion coefficients of solid cement paste at the nanoscopic scale. In the simplified criterion (14), the parameters T' and h' denotes the frictional and cohesion coefficients of the porous cement paste at the microscopic scale. That means that their values include implicitly the effect of nanoscopic pores on the strength properties of cement paste.

One considers again the uniaxial compression or tension test. At the failure state, the strength criterion (14) becomes:

$$\left(\frac{A' + \frac{2B'\rho}{3}}{1 + \frac{3\rho}{2} - \frac{5\rho}{6\left(\frac{A'}{B'} + 1\right)}} + \frac{B'}{9}\right)R^2 - \frac{C'}{3}R - \left(D' + \frac{4B'D' + C'^2}{6A'}\rho\right) = 0 \quad (16)$$

Two solutions of this equation correspond to the uniaxial tensile strength R_t and compressive strength R_c. These two macroscopic strength coefficients are functions of the microstructural parameters ρ, ϕ and the microscopic strength parameters T', h'. The inverse problem to be solved here is the determination of two microscopic strength parameters T', h' from the known values of microstructural parameters ρ, ϕ and the macroscopic strength properties (R_c, R_t), which can be easily measured by standard testing methods. This is a strongly nonlinear problem which is solved by an ANN-based method in this study.

3. Main steps of building an ANN model

The ANN originated from the biological nervous system and is optimized and applied to the deep learning algorithms (McCulloch and Pitts, 1943). The basic ANN is composed of artificial neurons connected to each other. The connections between neurons are used to transmit signals (called synapses). Each neuron first receives signals, then processes them, and finally sends signals to the neurons connected to it. Such ANNs are able to learn from observational data in the so-called training process and then to predict unknown results. The use of ANNs provides an efficient way to solve large size regression or classification problems. In this section, the main steps of establishing an ANN model are introduced.

Depending on the physical problems and the selected hyper-parameters, the original dataset is generally divided into three parts (train dataset, validation dataset, and test dataset) (Frank et al., 2014). The three parts of dataset are introduced into the model for training and testing. If the test results are satisfactory, the training ends. Otherwise, it is decided to continue the training process to optimize the hyper-parameters of the model, and the amount of original data can be increased if possible. The flowchart for building an ANN model is illustrated in Fig. 4.

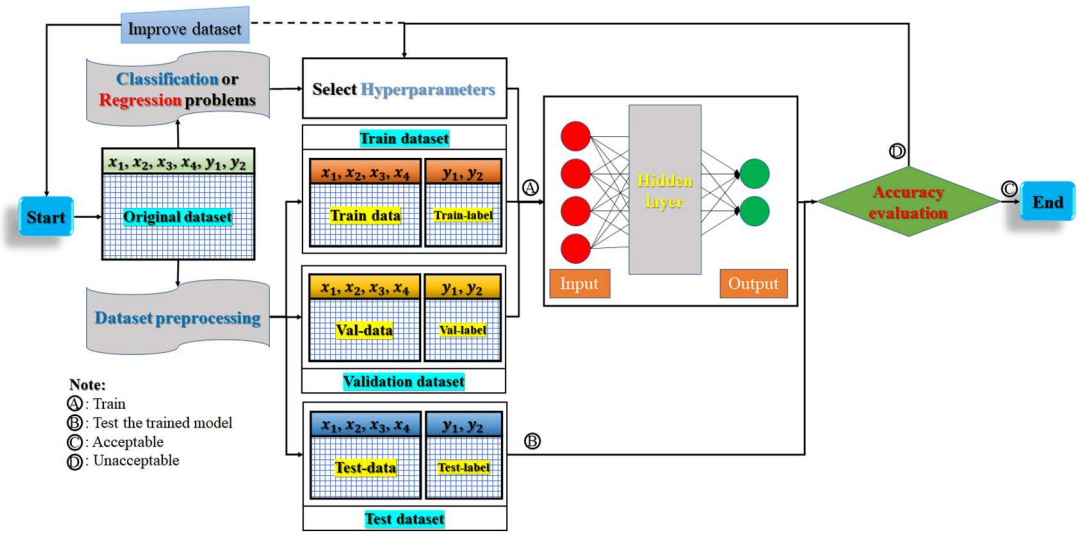

Fig. 4. Flowchart for building an ANN model

3.1 Original dataset preprocessing

The ANN modeling is based on the dataset, which is composed of input-data and output-label. The classification of input and output is determined according to the physical nature of problem. Meanwhile, it is difficult to obtain an accurate training model for different scales of input data (Haykin, 2010). Therefore, the preprocessing of the original data is very important to the modelling.

The preprocessing of the dataset includes two parts in general, one is the reasonable division of the dataset, and the other is the normalization or standardization of the dataset. The division of the dataset is mainly to complete the training and testing of the model, the commonly used allocation ratio is 60%, 20% and 20% for train, validation and test respectively (Hashemi et al., 2020; Jiang et al., 2020). The normalization or standardization of input and output data is to prevent overriding between different scales of numbers and premature saturation of hidden nodes (Haykin, 2010). This is completed by using Equation (17) (Ozgoren et al. 2013; Jiang et al., 2020) or (18) (Ciaburro et al., 2020):

$$x_i = 0.8\left(\frac{k_i - k_{min}}{k_{max} - k_{min}}\right) + 0.1 \tag{17}$$

where i, k_i, x_i, k_{max}, k_{min} are the serial number of the dataset, the actual value of the data, the normalized value, the maximum and minimum values of k_i in the data samples, respectively.

$$x_i = \frac{k_i - \mu}{\sigma} \tag{18}$$

where μ and σ are the mean and standard deviation in the data samples, respectively.

For the convenience of description, one takes 4-inputs and 2-outputs containing 10,000 series of original dataset as an example. This does not lose generality. In the beginning, the original dataset ($10k \times 6$ represents 10,000 rows and 6 columns) is randomly divided into two groups, one is the train group ($8k \times 6$), the other is the test group ($2k \times 6$). Subsequent, split the train group into two parts train-data (input parameters: $8k \times 4$) and train-label (output parameters: $8k \times 2$). Similarly, the test group also turns into two parts, namely, test-data ($2k \times 4$) and test-label ($2k \times 2$). Besides, Eq. (17) or (18) is used to normalize the train-data and test-data of the

previous step. It is worth noticing that the train-label and test-label do not need to be normalized. At the last, to make the prediction results of the model more accurate, 10,000 sets of data are selected from the train-label and the normalized train-data to make up a validation dataset, which is composed of validation-data ($2k \times 4$) and validation-label ($2k \times 2$). In this way, the required train dataset, validation dataset, and test dataset are obtained. The detailed steps are indicated in Fig. 5. The data set used in this study can be found in the shared file mentioned in the Supplementary Information at the end of this paper.

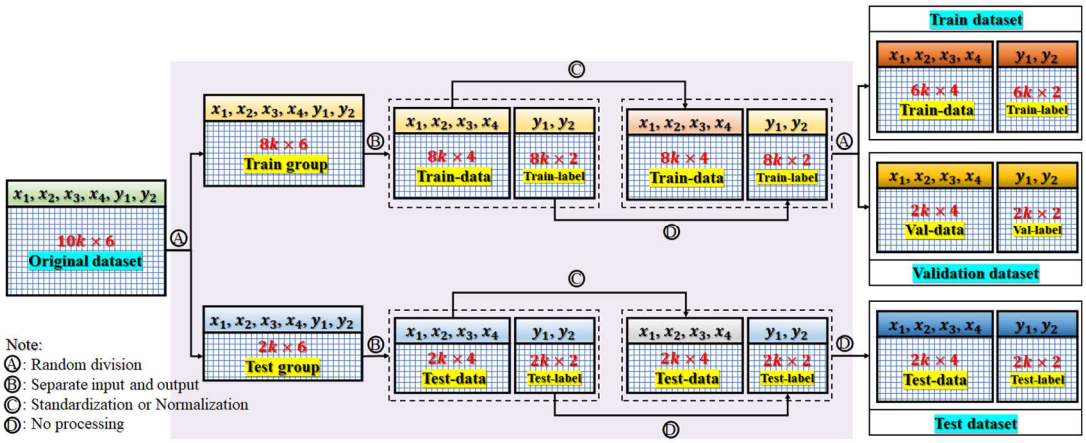

Fig. 5 Original dataset preprocessing process

3.2 Determination of network structure and algorithm

There are several types of ANNs such as feed-forward, radial basis function, and recurrent neural networks. For most engineering problems (Ghritlahre and Prasad, 2018; Jiang et al., 2020; Guijo-Rubio et al., 2020, Shen et al., 2020), the most commonly used one is the feed-forward neural network structure with the back-propagation (BP) algorithm (Fig. 6). The BP neural network is then adopted in this study.

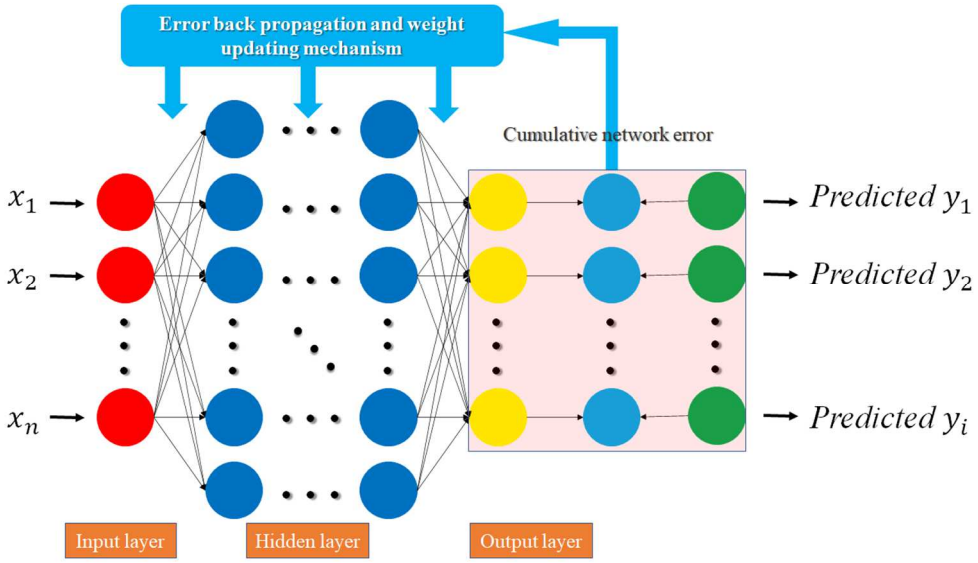

Fig. 6. A multi-layer feed-forward ANN model with a back-propagation algorithm

348

349 A neural network has multiple layers, including one input, one output, and one or
350 more hidden layers with a specific number of neurons in each layer. The neurons in
351 each layer have two functions: the summation and activation, which are used to sum
352 the weighted inputs and to activate this summation to produce the outputs,
353 respectively. The internal structure of a neuron is described in Fig. 7. The l-th layer
354 has n neurons while the $(l-1)$-th layer has m neurons. The input/output relationship
355 of a neuron is indicated in a matrix form as follows:

$$a_i^l = \sigma\left(\sum_{j=1}^{m} \boldsymbol{w}_{ij}^l \, \boldsymbol{a}_j^{l-1} + \boldsymbol{b}_i^l\right) \tag{19}$$

356 where $\boldsymbol{w}_{ij}^l$ is the weight matrix from the $(l-1)$-th layer to the l-th layer, $\boldsymbol{b}_i^l$ is the
357 bias vector for inputs on the l-th layer, The indices range $i = 1,2,\ldots,n$, and $j =$
358 $1,2,\ldots,m$. σ represents the activation function. The most widely used activation
359 functions are: $\sigma(x) = tanhx$ (hyperbolic tangent), $\sigma(x) = \max(0,x)$ (ReLU),
360 $\sigma(x) = \frac{1}{1+\exp(-x)}$ (Sigmoid), $\sigma(x) = In(1+\exp x)$ (Softplus) and $\sigma(x) = x$
361 (linear) etc. It is worth noticing that the values of weight coefficient and bias are
362 essential for the ANN based simulation. Detailed and interesting discussions on this
363 aspect have been presented in some recent studies (Asteris and Mokos, 2020; Le at al.,
364 2021; Asteris et al., 2021; Armaghani et al., 2021). However, it is not easy to present

their values directly in the paper. The values of weights and bias used in the present study are given in the shared file mentioned in the Supplementary Information at the end of the paper.

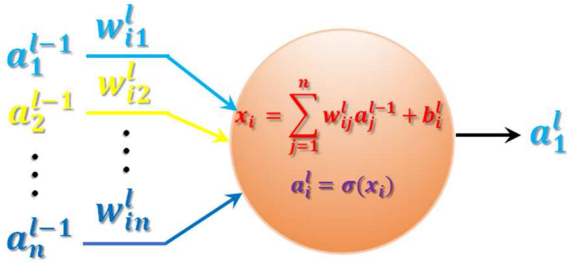

Fig. 7. Artificial neuron

After the network is established, the model needs to be trained with the preprocessed dataset to achieve the target output. The training process is through adjusting the weights and bias of the network to obtain minimizing the defined loss function (or cost function), e.g., the mean squared error (MSE) defined in Eq. (20) (Ashrafian et al., 2020) between the target output and the predicted output for regression problems. At the validation phase, the mean absolute error (MAE) defined in Eq. (21) (Ashrafian et al., 2020) is used.

$$MSE = \frac{1}{n}\sum_{i=1}^{n}[\ f(x_i)\ -\ y_i\ ]^2 \quad (20)$$

$$MAE = \frac{1}{n}\sum_{i=1}^{n}|f(x_i)\ -\ y_i\ | \quad (21)$$

in which $f(x_i)$ denotes the ANN prediction, y_i is the true value. Note that in order to speed up the training procedure, the gradient of loss function over all the training inputs will be approximated by the one over a small number batch-size (mini-batch), randomly chosen from training data.

In the BP neural network with a gradient-based optimization algorithm, the cumulative network error between its final output and the actual value is back-propagated to quickly adjust the values of the weights in the whole network as shown in Fig. 6. For more theoretical details about ANN training, readers can refer to some reference literatures (Hassan et al., 2009; Deo and Sahim, 2015; Ghritlahre and

Prasad, 2018; Ford et al. 2020; Hashemi et al., 2020; Guijo_Rubio et al., 2020; Delgado et al., 2020; Ghorpade et al., 2020; Hegde and Rokseth, 2020). In this paper, the algorithm for first-order gradient-based optimization of stochastic objective functions is adopted (Chang et al., 2019). It is based on adaptive estimates of lower-order moments:

$$g_t = \nabla_\theta \ J(\theta_{t-1}),\ m_t = \beta_1 m_{t-1} + (1-\beta_1)\ g_t,$$
$$v_t = \beta_2 v_{t-1} + (1-\beta_2) g_t^2,\ \widehat{m}_t = \frac{m_t}{1-\beta_1^t},\ \widehat{v}_t = \frac{v_t}{1-\beta_2^t},\ \theta_t = \theta_{t-1} - \frac{\alpha \times \widehat{m}_t}{\sqrt{\widehat{v}_t}+\varepsilon}. \quad (22)$$

where m_t and v_t are the first-order and second-order momentum. β_1 and β_2 are their exponential decay rate while $\widehat{m}_t$ and $\widehat{v}_t$ are the corresponding modifications of m_t and v_t. α indicates the learning rate. ε is a very small constant to avoid denominator to be zero.

3.3 Verification of the trained ANN model

The test datasets are used to verify the prediction ability of the optimized ANN model. To have a more comprehensive and better comparison, some statistical error analysis parameters are used as criteria to evaluate the model.

The important statistical parameters used in this study include the relative error (RE), absolute relative error (ARE), average absolute relative error (AARE), maximum absolute relative error (Max-ARE), and coefficient of determination (R^2) (Hashemi et al., 2020). These parameters can be calculated as follows:

$$\mu_i = \frac{x_{ipr} - x_{iac}}{x_{iac}} \times 100\% \quad (23)$$

$$\mu_{ia} = |\mu_i| \quad (24)$$

$$\bar{\mu} = \frac{\sum_{i=1}^{n} \mu_{ia}}{n} \quad (25)$$

$$\mu_{max} = \max(\mu_{ia}) \quad (26)$$

$$R^2 = 1 - \frac{\sum_{i=1}^{n} (x_{iac} - x_{ipr})^2}{\sum_{i=1}^{n} (x_{ipr} - \bar{x})^2},\ \bar{x} = \frac{\sum_{i=1}^{n} x_{iac}}{n} \quad (27)$$

In these relations, x_{iac} represents i-th actual value, x_{ipr} represents i-th predicted value, μ_i represents i-th RE, μ_{ia} represents i-th ARE, $\bar{\mu}$ represents AARE, μ_{max} represents Max-ARE.

4. An ANN model to estimate T' and h'

This section describes the building of an ANN method based model to predict T' and h' and the evaluation of the developed model.

4.1 Original dataset source

Based on Eq. (16), the purpose here is to generate the dataset $(\rho, \phi, T', h', R_c, R_t)$. In this study, a loop algorithm is used to generate 10,000 sets of data. The core steps of the calculation are as follows.

Step 1: Randomly assign values to the four parameters (ρ, ϕ, T', h') respectively. The selected value ranges are $\rho\epsilon[0,1]$, $\phi\epsilon[0,1]$, $T'\epsilon[0,1]$, $h'\epsilon[0,80]$. Then, go to step 2.

Step 2: Check whether each set assigned in the step 1 meets the requirement that the denominator is not zero for the mathematical definition. Here one refers to: $T' \neq 0$, $4T'^2 - 9 \neq 0$, $A' \neq 0$, $B' \neq 0$, $\frac{A'}{B'} + 1 \neq 0$, $1 + \frac{3\rho}{2} - \frac{5\rho}{6\left(\frac{A'}{B'}+1\right)} \neq 0$. If it meets the mathematical conditions, go to step 3, otherwise return to step 1.

Step 3: Bring the sets that meet the requirements in step 2 into Eq. (16) and solve it. Then, go to step 4.

Step 4: Judge if the product of the two roots in step 3 is less than 0 (It is stipulated that the compressive strength value is positive and the tensile strength value is negative in Eq. (16), so the solution of the equation must be one positive and one negative). If the product is less than 0, go to step 5, else return to step 1.

Step 5: The positive roots of Eq. (16) solved in step 4 are assigned to compressive strength R_c, while the absolute value of negative root is assigned to tensile strength R_t. Then, go to step 6.

Step 6: Check whether each value of R_c and R_t respectively meets: $1 < R_c < 100$ and $\frac{1}{20} * R_c < R_t < \frac{1}{10} * R_c$ (for most ordinary concrete materials, the compressive strength is generally between 1 to 100 MPa, and the tensile strength is $\frac{1}{20}$-$\frac{1}{10}$ times the compressive strength (Gaedicke at al., 2020)). If yes, print $\rho, \phi, T', h', R_c, R_t$;

Else, return to step 1.

The flowchart for generating the dataset is shown in Fig. 8. A Python script was developed to automate the collection of data through the above process.

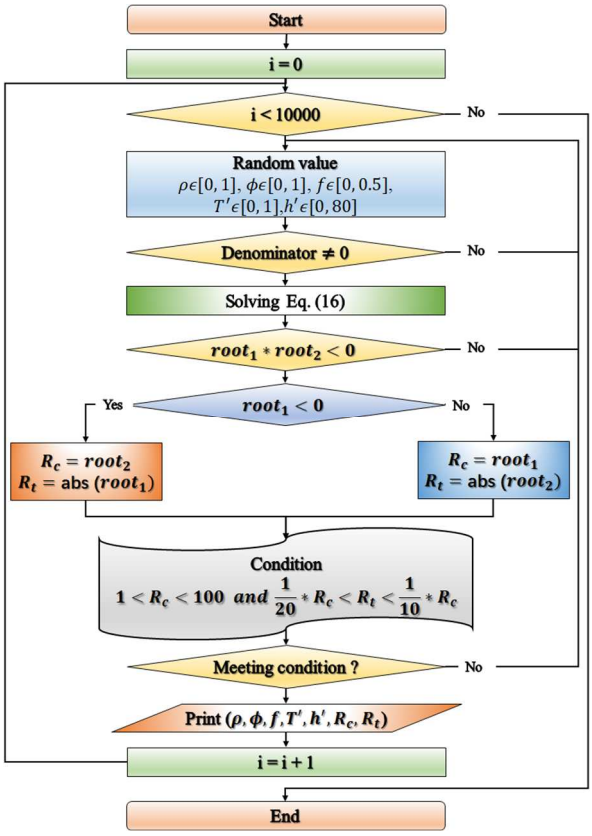

Fig. 8 The flowchart for data generation

4.2 Construction of the ANN model

In this study, an advanced open-source neural network library Keras (2020) is used to train the ANN model, able to run on TensorFlow (by Google), CNTK (by Microsoft), or Theano (Team et al., 2016). TensorFlow is employed in this work to solve the regression problem consisting in predicting the values of T' and h'. A BP neural network with four hidden layers and 100 neurons in each is constructed. The network structure is shown in Fig. 9. It is important to outpoint that the choice of ANN architecture is the first important step in developing an ANN model that best suits the problem in hand. Unfortunately, there is no guidance for selecting the optimal ANN architecture. For instance, the number of layers and neurons are two hyper-parameters of the model, which cannot be learnt during the training process. In

the present work, inspired by previous studies on similar problems (Asteris and Plevris, 2017; Asteris and Mokos, 2020; Ford et al. 2020; Konstantopoulos et al., 2020), preliminary calculations were performed by taking different numbers of layers and neurons. The accuracy and loss function were compared. Based on such comparisons, the ANN architecture shown in Fig. 9 is chosen. As it will be shown in Section 4.3, this architecture provides a very high accuracy. The input/output data and hyper-parameters for this study are presented in Table 1. The MSE is used as the loss function and the Adam ($\beta_1 = 0.9,\ \beta_2 = 0.999,\ \alpha = 0.001,\ \varepsilon = 10\mathrm{e}^{-8}$) is adopted as the optimizer. The training and validation processes are illustrated in terms of the MAE. Further, the Batch-size is 50 and maximum number of epochs is 10,000 for training.

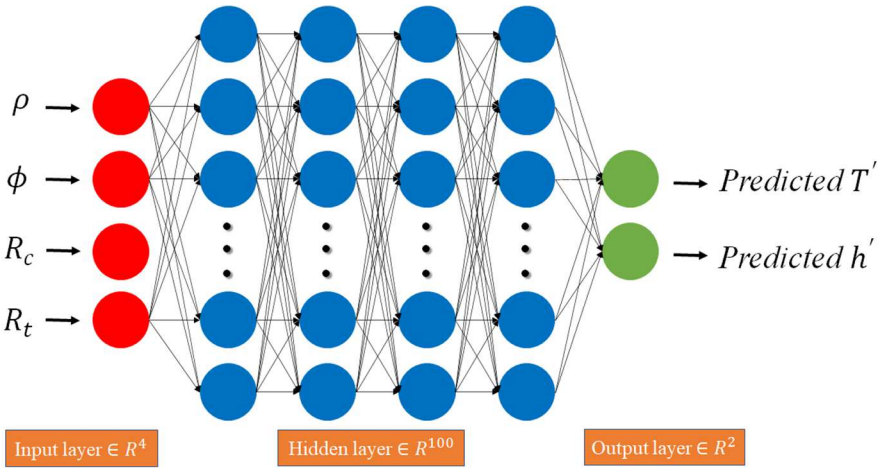

Fig.9. Established BP neural network model

Table 1: Hyper-parameters of the ANN model for prediction of T' and h'

Input layer	Hidden layer	Output layer	Loss function	Optimizer
ρ, ϕ, R_c, R_t	$4 \times 100 \times$ ReLU	T', h'	MSE	Adam

Another important step for constructing an ANN model is the choice of activation function. As mentioned in sub-section 3.2, there are five widely used activation functions for ANN models. In order to make our choice, we have made preliminary calculations in order to compare these five functions, by using 6000 data sets for training, 2000 for validation and 2000 for test of the ANN model. It was seen that the output results of the activation functions ReLU, sigmoid and softplus were

among the best ones in terms of MAE, MSE and R^2. The differences between them were very small. The quality of two other functions was clearly below these three. As ReLU is well-known in literature and widely used in previous studies, it is taken in this work. It is a traditional and efficient activation function with two main advantages: more efficient gradient descent and back propagation, and simpler calculation process.

4.3 Verification of the trained model

The evolutions of the loss function and the MAE of the training set and the validation set in the training data are illustrated in Fig. 10 as functions of the number of epochs. It can be seen that the proposed neural network model converges very quickly. After continuous learning and self-adjustment of the network, the loss function drops rapidly. Simultaneously, the MAE is further reduced. The final values of MAE and loss function are 1.03625×10^{-3} and 2.05×10^{-6} for the training dataset and 8.18333×10^{-4}, 1.36×10^{-6} for the validation dataset.

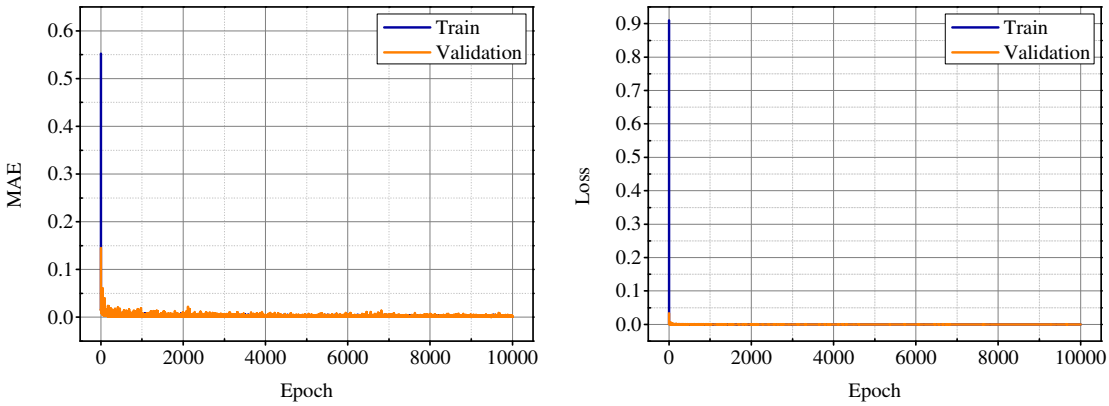

Fig. 10. MAE and loss function evolution during training process

In order to evaluate the accuracy of ANN-based model, in Fig. 11, one shows the relative errors of predicted T' and h' for 2,000 selected data. For the value of T', most of the relative errors are between ±0.15 while those of $h'$are between ±0.25. In Fig. 12, one plots the predicted values versus exact ones to visualize their correlations. Very high values of R^2 are obtained (0.997 for T' and 1 for h'). These results indicate the high prediction accuracy of the BP neural network model.

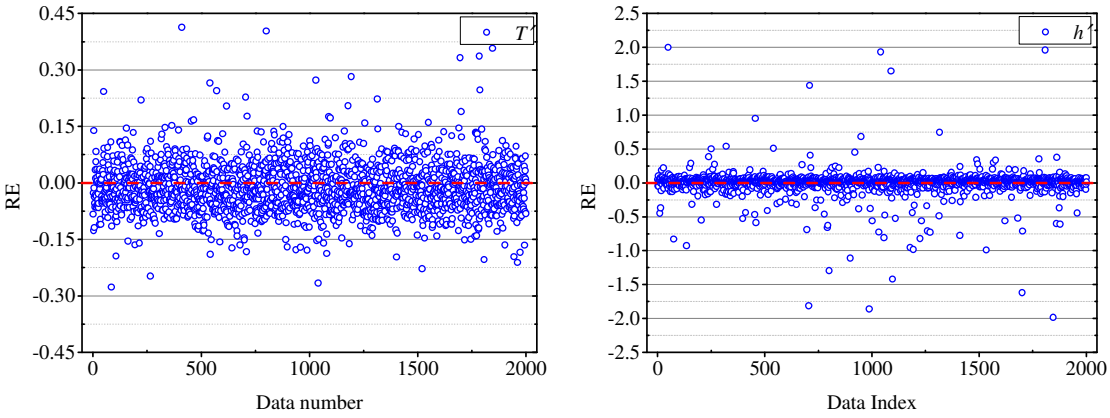

Fig. 11: Relative errors (RE) of predicted microscopic strength parameters

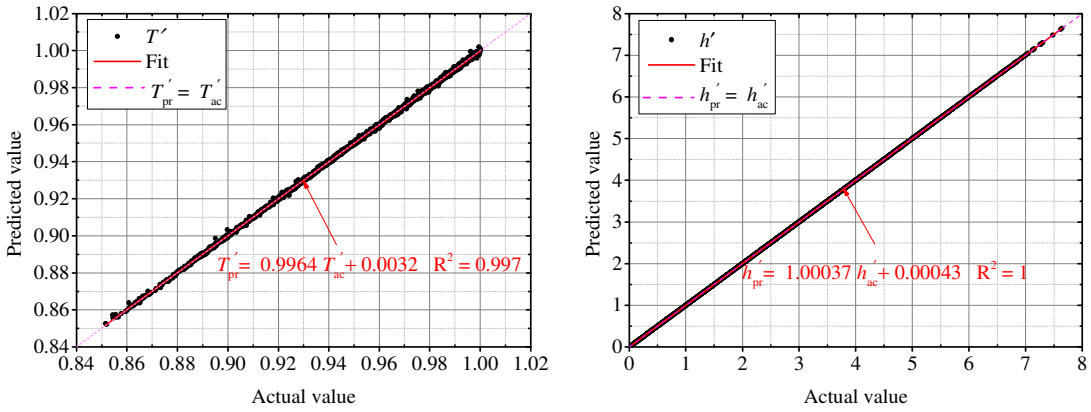

Fig. 12: Correlation between predicted and exact values of T' and h'

Further, in Fig. 13, one shows the direct comparisons between the predicted and exact values of T' and h' for 200 data sets, together with the relative errors (RE). It can be seen that for most of the selected data points, the relative errors are relatively small (except several noises). This again demonstrates that the BP neural network model has a high accuracy.

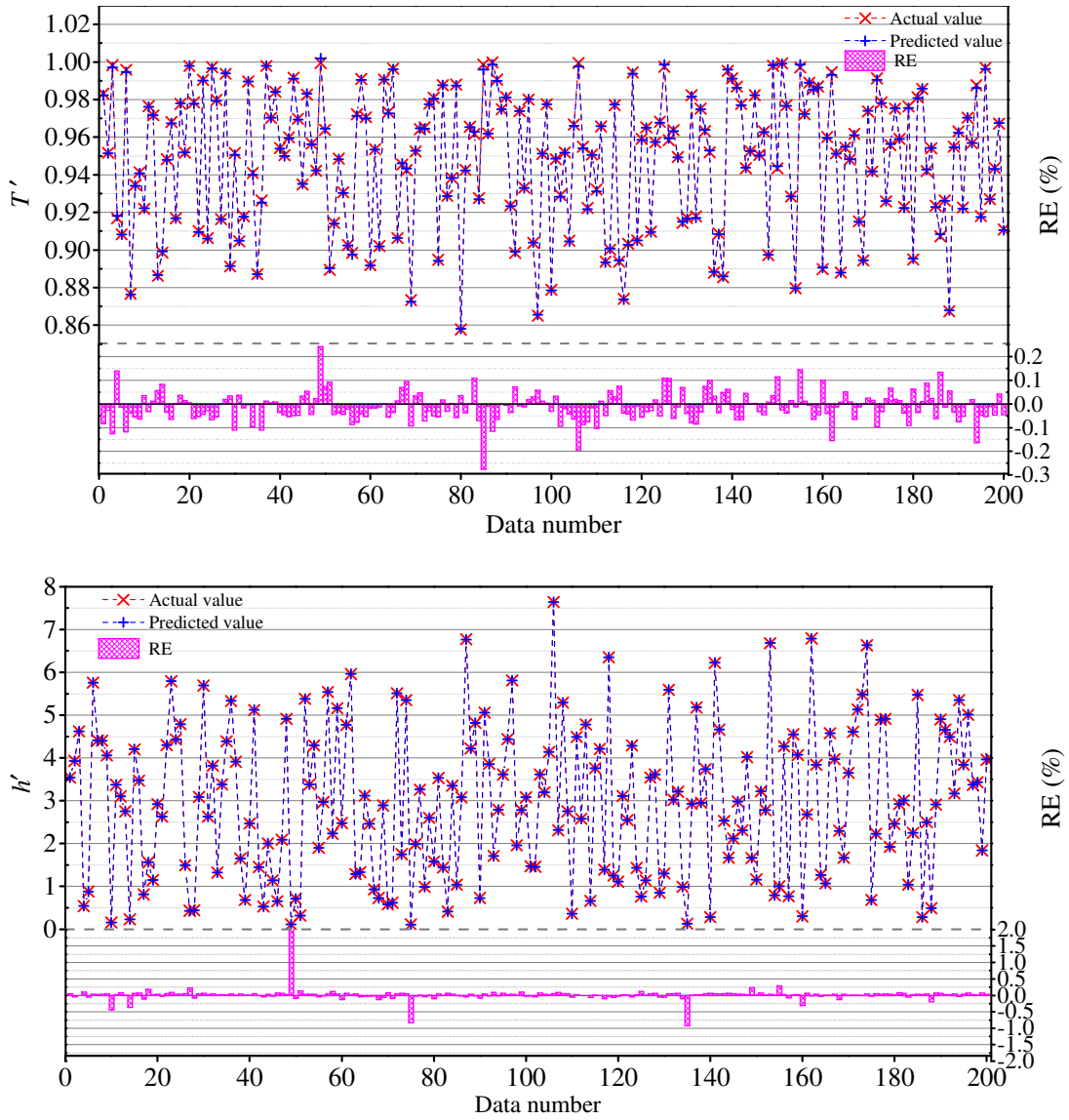

Fig. 13. Comparisons between predicted and exact values of T' and h' for 200 data sets

In order to better understand the error origin of the proposed model, more detailed analyses are presented in Fig. 14 and Fig. 15. From Fig. 14, one can see that the Max-ARE of T' and h' are 0.41% and 2.0%, and their AARE are 0.05% and 0.07%, respectively. In addition, ARE of T' is less than 0.13% for 95% of the data, and higher than 0.27% for only 0.5%. Similarly, ARE of h' is 1.42% for 95% of the data and 0.2% for only 0.5%. In Fig. 15, the values of ARE are classified in four levels respectively in terms of ARE > 1%, 0.5% < ARE < 1%, 0.2% < ARE < 0.5%, and ARE < 0.2%. The amount of data whose error is less than 1% occupies more than

99.4% for predicting T' and h'. There is an excellent predictive accuracy for the ANN-based model. The detailed comparisons between the test data obtained from the analytical strength criterion and the predicted values of friction T′ and cohesion h′ are also presented in the shared file mentioned in the Supplementary Information at the end of the paper.

However, it is worth noticing that for engineering application purpose, it would be necessary to check the accuracy of the ANN based method by comparing numerical predictions with experimental results. We recall that the main objective of the present work is to identify the microscopic strength parameters (friction and cohesion) of porous cements paste from the measured macroscopic strength parameters (uniaxial compression and tension strengths). Therefore, for a complete experimental validation, it is need to have a complete set of experimental data on concrete samples with known micro-structures for which both macroscopic and microscopic strength parameters are measured. Unfortunately, we do not have so far such data in hand. We shall take up this exciting challenge in future studies. Therefore, the accuracy of the proposed ANN based model is verified by comparisons with the analytical solutions.

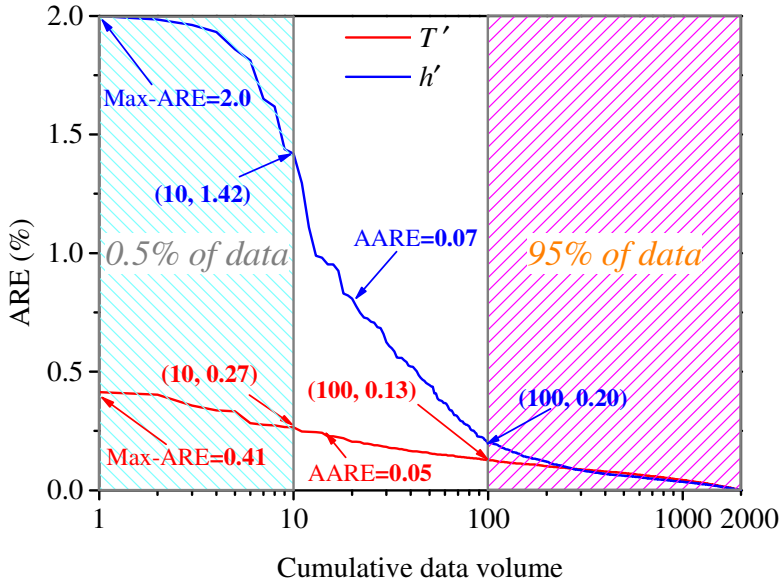

Fig. 14. ARE distribution of T' and h'

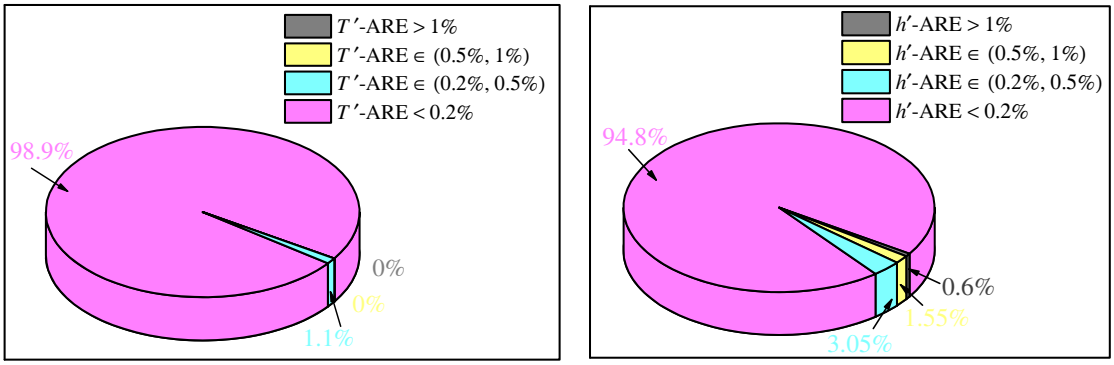

Fig. 15. Proportions of errors of T' and h' in terms of four levels of ARE

5. Conclusions

In this paper, an ANN based numerical method has been developed for identification of microscopic strength properties of concrete-like composites. This method can be also applied to other types of heterogeneous materials. Therefore, this machine-learning method provides an efficient way for the calibration of local properties of constituent phases at different scales, a crucial challenge of multi-scale modeling of heterogeneous materials.

In the present study, the dataset used for training and validation was generated with the help of a close-form strength criterion issued from an analytical homogenization procedure. This dataset can be enriched by any other kinds of data, either from direct numerical simulations of micro-structures or experimental tests.

In the case considered here, the proposed method has shown a very good accuracy for the prediction of frictional coefficient and cohesion of cement paste at the microscopic scale. The ANN model contained a BP algorithm and four hidden layers with 100 neurons in each one. With a database of 10,000 sets, the probability of the absolute relative error (ARE) of less than 1% exceeds 99%.

In future studies, with the enrichment of dataset by adding results from direct simulations of different types of micro-structures, in particular by considering ITZ, it will be possible to directly evaluate macroscopic mechanical properties of concrete materials, for which any analytical homogenization solutions cannot be found. Also, with the ANN based inverse optimization method proposed here, it will be also identify local mechanical properties of constituents in complex micro-structural

morphology such as those of ITZ. As an exciting challenge, the efficiency of the proposed ANN based method can also be verified by suitable experimental data. For this purpose, multi-scale laboratory tests should be performed on typical concrete samples with controlled micro-structures (porosity, mineral compositions, morphology) for which both macroscopic and microscopic mechanical properties can be measured.

Acknowledgements:

The scholarship provided by the China Scholarship Council (CSC, grant No. 201908230319) to the first author is gratefully acknowledged.

References:

1. F. Aldakheel, A microscale model for concrete failure in poro-elasto-plastic media, Theoretical and Applied Fracture Mechanics 107 (2020) 102517
2. Apostolopoulou, M., Asteris, P.G., Armaghani, D.J., Douvika, M.G., Lourenço, P.B., Cavaleri, L., Bakolas, A., Moropoulou, A., Mapping and holistic design of natural hydraulic lime mortars, Cement and Concrete Research, 136 (2020), 106167
3. Armaghani, D.J., Mamou, A., Maraveas, C., Roussis, P.C., Siorikis, V.G., Skentou, A.D. and Asteris, P.G., Predicting the unconfined compressive strength of granite using only two non-destructive test indexes, Geomechanics and Engineering 25(4) (2021): 317-330
4. A. Ashrafian, F. Shokri, M.J. Taheri Amiri, Z.M. Yaseen, M. Rezaie-Balf, Compressive strength of Foamed Cellular Lightweight Concrete simulation: New development of hybrid artificial intelligence model, Construction and Building Materials 230 (2020) 117048
5. Asteris, P.G., Plevris, V., Anisotropic Masonry Failure Criterion Using Artificial Neural Networks, Neural Computing and Applications, 28 (8) (2017): 2207-2229
6. Asteris, P.G., Moropoulou, A., Skentou, A.D., Apostolopoulou, M., Mohebkhah, A., Cavaleri, L., Rodrigues, H., Varum, H. (2019). Stochastic vulnerability assessment of masonry structures: Concepts, modeling and restoration Aspects, Appl. Sci., 9(2) (2019), 243
7. Asteris, P.G., Mokos, V.G., Concrete Compressive Strength using Artificial Neural Networks, Neural Computing and Applications, 32 (2020), 1807-1826
8. Asteris, P.G., Skentou, A.D., Bardhan, A., Samui, P., Pilakoutas, K., Predicting concrete compressive strength using hybrid ensembling of surrogate machine learning models, Cement and Concrete Research, 145 (2021), 106449

9. Asteris, P.G., Lemonis, M.E., Nguyen, T.A., Van Le, H., Pham, B.T., Soft computing-based estimation of ultimate axial load of rectangular concrete-filled steel tubes, Steel and Composite Structures 39(4) (2021), 471
10. F. Bignonnet, L. Dormieux, D. Kondo, A micro-mechanical model for the plasticity of porous granular media and link with the Cam clay model, International Journal of Plasticity 79 (2016) 259-274.
11. D.G. Cacuci, M. Ionescu-Bujor, I.M. Navon, Sensitivity and uncertainty analysis, volume II: applications to large-scale systems, CRC press2005.
12. Y.J. Cao, W.Q. Shen, J.F. Shao, N. Burlion, Influences of micro-pores and meso-pores on elastic and plastic properties of porous materials, European Journal of Mechanics - A/Solids 72 (2018) 407-423.
13. Y.J. Cao, W.Q. Shen, N. Burlion, J.F. Shao, Effects of inclusions and pores on plastic and viscoplastic deformation of rock-like materials, International Journal of Plasticity 108 (2018) 107-124.
14. Y.J. Cao, W.Q. Shen, J.F. Shao, W. Wang, A novel FFT-based phase field model for damage and cracking behavior of heterogeneous materials, International Journal of Plasticity 133 (2020) 102786.
15. Y.J. Cao, W.Q. Shen, J.F. Shao, W. Wang, A multi-scale model of plasticity and damage for rock-like materials with pores and inclusions, online, Int. J. Rock Mechanics and Mining Science
16. Z. Chang, Y. Zhang, W. Chen, Electricity price prediction based on hybrid model of adam optimized LSTM neural network and wavelet transform, Energy 187 (2019) 115804.
17. S.J. Chen, W.H. Duan, Z.J. Li, T.B. Sui, New approach for characterisation of mechanical properties of cement paste at micrometre scale, Materials & Design 87 (2015) 992-995.
18. G. Ciaburro, G. Iannace, M. Ali, A. Alabdulkarem, A. Nuhait, An artificial neural network approach to modelling absorbent asphalts acoustic properties, Journal of King Saud University - Engineering Sciences (2020).
19. V. Czitrom, One-Factor-at-a-Time versus Designed Experiments, The American Statistician 53(2) (1999) 126-131.
20. J.M.P.Q. Delgado, F.A.N. Silva, A.C. Azevedo, D.F. Silva, R.L.B. Campello, R.L. Santos, Artificial neural networks to assess the useful life of reinforced concrete elements deteriorated by accelerated chloride tests, Journal of Building Engineering 31 (2020) 101445.
21. R.C. Deo, M. Sahin, Application of the Artificial Neural Network model for prediction of monthly Standardized Precipitation and Evapotranspiration Index using hydrometeorological parameters and climate indices in eastern Australia, Atmospheric Research 161-162 (2015) 65-81.
22. E. Ford, S. Kailas, K. Maneparambil, N. Neithalath, Machine learning approaches to predict the micromechanical properties of cementitious hydration phases from microstructural chemical maps, Construction and Building Materials 265 (2020) 120647.

23. H. Frank, H. Holger, L.-B. Kevin, An Efficient Approach for Assessing Hyperparameter Importance, PMLR, 2014, pp. 754-762.
24. C. Gaedicke, A. Torres, K.C.T. Huynh, A. Marines, A method to correlate splitting tensile strength and compressive strength of pervious concrete cylinders and cores, Construction and Building Materials 125 (2016) 271-278.
25. F. Galton, Kinship and Correlation, Statist. Sci. 4(2) (1989) 81-86.
26. H.K. Ghritlahre, R.K. Prasad, Exergetic performance prediction of solar air heater using MLP, GRNN and RBF models of artificial neural network technique, Journal of environmental management 223 (2018) 566-575.
27. Ghorbanbeigi, H., Shen, W.Q., Yurtdas, I., Shao, J.F., A micro-mechanics based model for concrete materials subjected to carbonation, International Journal for Numerical and Analytical Methods in Geomechanics 40(2016): 1203-1218
28. V.G. Ghorpade, V.S. Koneru, Pattern recognition neural network model for experimental based compressive strength graded self compacting concrete, Materials Today: Proceedings (2020).
29. A. Griewank, A. Walther, Evaluating derivatives: principles and techniques of algorithmic differentiation, SIAM2008.
30. D. Guijo-Rubio, A.M. Durán-Rosal, P.A. Gutiérrez, A.M. Gómez-Orellana, C. Casanova-Mateo, J. Sanz-Justo, S. Salcedo-Sanz, C. Hervás-Martínez, Evolutionary artificial neural networks for accurate solar radiation prediction, Energy 210 (2020) 118374.
31. A. Hashemi Fath, F. Madanifar, M. Abbasi, Implementation of multilayer perceptron (MLP) and radial basis function (RBF) neural networks to predict solution gas-oil ratio of crude oil systems, Petroleum 6(1) (2020) 80-91.
32. A.M. Hassan, A. Alrashdan, M.T. Hayajneh, A.T. Mayyas, Prediction of density, porosity and hardness in aluminum–copper-based composite materials using artificial neural network, Journal of Materials Processing Technology 209(2) (2009) 894-899.
33. S. Haykin, Neural Networks and Learning Machines, 3/E, Pearson Education India2010.
34. J. Hegde, B. Rokseth, Applications of machine learning methods for engineering risk assessment – A review, Safety Science 122 (2020) 104492.
35. M.J.W. Jansen, Analysis of variance designs for model output, Computer Physics Communications 117(1) (1999) 35-43.
36. H. Jiang, Z. Xi, A. A. Rahman, X. Zhang, Prediction of output power with artificial neural network using extended datasets for Stirling engines, Applied Energy 271 (2020) 115123.
37. keras, 2020. https://keras.io/.
38. M. Königsberger, M. Hlobil, B. Delsaute, S. Staquet, C. Hellmich, B. Pichler, Hydrate failure in ITZ governs concrete strength: A micro-to-macro validated engineering mechanics model, Cement and Concrete Research 103 (2018) 77-94.
39. G. Konstantopoulos, E.P. Koumoulos, C.A. Charitidis, Testing Novel Portland Cement Formulations with Carbon Nanotubes and Intrinsic Properties Revelation:

Nanoindentation Analysis with Machine Learning on Microstructure Identification, Nanomaterials 10(4) (2020).
40. C.K. Lau, H. Lee, V. Vimonsatit, W.Y. Huen, P. Chindaprasirt, Abrasion resistance behaviour of fly ash based geopolymer using nanoindentation and artificial neural network, Construction and Building Materials 212 (2019) 635-644.
41. Le, T.T., Asteris, P.G., Lemonis, M.E., Prediction of axial load capacity of rectangular concrete-filled steel tube columns using machine learning techniques, Engineering with Computers (2021), in press, https://doi.org/10.1007/s00366-021-01461-0
42. S. Maghous, L. Dormieux, J.F. Barthélémy, Micromechanical approach to the strength properties of frictional geomaterials, European Journal of Mechanics - A/Solids 28(1) (2009) 179-188.
43. W.S. McCulloch, W. Pitts, A logical calculus of the ideas immanent in nervous activity, The bulletin of mathematical biophysics 5(4) (1943) 115-133.
44. J. Nemecek, V. Králík, V. Šmilauer, L. Polívka, A. Jäger, Tensile strength of hydrated cement paste phases assessed by micro-bending tests and nanoindentation, Cement and Concrete Composites 73 (2016) 164-173.
45. Y.O. Ozgoren, S. Cetinkaya, S. Sarıdemir, A. Cicek, F. Kara, Predictive modeling of performance of a helium charged Stirling engine using an artificial neural network, Energy Conversion and Management 67 (2013) 357-368.
46. P. Paruolo, M. Saisana, A. Saltelli, Ratings and rankings: voodoo or science?, Journal of the Royal Statistical Society: Series A (Statistics in Society) 176(3) (2013) 609-634.
47. H. Paiva, A.S. Silva, A. Velosa, P. Cachim, V.M. Ferreira, Microstructure and hardened state properties on pozzolan-containing concrete, Construction and Building Materials 140 (2017) 374-384.
48. R. Qian, Y. Zhang, C. Liu, L. Yang, G. Liu, W. She, Quantitative characterization of three-dimensional pore structure in hardened cement paste using X-ray microtomography combined with centrifuge driven metal alloy intrusion, Materials Characterization 145 (2018) 277-283.
49. A.A. Rahman, X. Zhang, Prediction of oscillatory heat transfer coefficient for a thermoacoustic heat exchanger through artificial neural network technique, International Journal of Heat and Mass Transfer 124 (2018) 1088-1096.
50. S. Razavi, H.V. Gupta, A new framework for comprehensive, robust, and efficient global sensitivity analysis: 1. Theory, Water Resources Research 52(1) (2016) 423-439.
51. S. Razavi, H.V. Gupta, A new framework for comprehensive, robust, and efficient global sensitivity analysis: 2. Application, Water Resources Research 52(1) (2016) 440-455.
52. A. Saltelli, P. Annoni, How to avoid a perfunctory sensitivity analysis, Environmental Modelling & Software 25(12) (2010) 1508-1517.

53. A. Saltelli, P. Annoni, I. Azzini, F. Campolongo, M. Ratto, S. Tarantola, Variance based sensitivity analysis of model output. Design and estimator for the total sensitivity index, Computer Physics Communications 181(2) (2010) 259-270.
54. A. Saltelli, Making best use of model evaluations to compute sensitivity indices, Computer Physics Communications 145(2) (2002) 280-297.
55. W.Q. Shen, Y.J. Cao, J.F. Shao, Z.B. Liu, Prediction of plastic yield surface for porous materials by a machine learning approach, Materials Today Communications 25 (2020) 101477.
56. W.Q. Shen, D. Kondo, L. Dormieux, J.F. Shao, A closed-form three scale model for ductile rocks with a plastically compressible porous matrix, Mechanics of Materials 59 (2013) 73-86.
57. W.Q. Shen, J.F. Shao, An incremental micro-macro model for porous geomaterials with double porosity and inclusion, International Journal of Plasticity 83 (2016) 37-54.
58. W.Q. Shen, J.F. Shao, Y.J. Cao, S.S. Wang, W.Y. Xu, A micromechanics-based enhanced plastic damage model including localization analysis for heterogeneous geomaterials, Computers and Geotechnics 122 (2020) 103512.
59. W.Q. Shen, J.F. Shao, D. Kondo, B. Gatmiri, A micro–macro model for clayey rocks with a plastic compressible porous matrix, International Journal of Plasticity 36 (2012) 64-85.
60. W.Q. Shen, J.F. Shao, Z.B. Liu, A. Oueslati, G. De Saxcé, Evaluation and improvement of macroscopic yield criteria of porous media having a Drucker-Prager matrix, International Journal of Plasticity 126 (2020) 102609.
61. W.Q. Shen, J. Zhang, J.F. Shao, D. Kondo, Approximate macroscopic yield criteria for Drucker-Prager type solids with spheroidal voids, International Journal of Plasticity 99 (2017) 221-247.
62. Shen WQ, Cao YJ, Liu ZB, Shao JF (2020), A multiscale elastoplastic constitutive model for geomaterials with a porous matrix-inclusion microstructure, Computers and Geotechnics 126, doi.org/10.1016/j.compgeo.2020.103683
63. Z. Shen, Y. Bi, Y. Wang, C. Guo, MLP neural network-based recursive sliding mode dynamic surface control for trajectory tracking of fully actuated surface vessel subject to unknown dynamics and input saturation, Neurocomputing 377 (2020) 103-112.
64. T. Team, R. Al-Rfou, G. Alain, A. Almahairi, C. Angermueller, D. Bahdanau, N. Ballas, F. Bastien, J. Bayer, A. Belikov, A. Belopolsky, Y. Bengio, A. Bergeron, J. Bergstra, V. Bisson, J. Bleecher Snyder, N. Bouchard, N. Boulanger-Lewandowski, X. Bouthillier, Y. Zhang, Theano: A Python framework for fast computation of mathematical expressions, (2016)
65. Zeng, J., Roussis, P.C., Mohammed, A.S., Maraveas, C., Fatemi, S.A., Armaghani, D.J., Asteris, P.G., Prediction of Peak Particle Velocity Caused by Blasting through the Combinations of Boosted-CHAID and SVM Models with Various Kernels. Appl. Sci. 11 (2021), 3705

66. H. Zhang, Y. Xu, Y. Gan, Z. Chang, E. Schlangen, B. Savija, Microstructure informed micromechanical modelling of hydrated cement paste: Techniques and challenges, Construction and Building Materials 251 (2020) 118983.